Advanced Ceramics Progress: Vol. 11, No. 3, (Summer 2025) 1-12

Materials and Energy Research Center
MERC

Contents lists available at ACERP

Advanced Ceramics Progress

Journal Homepage: www.acerp.ir

**Original Research Article**

# The Effect of Metallic and Oxide Additives on Spark Plasma Sintering and Properties of Silicon Carbide Components

Mohamadreza Falah[a], Mahdi Shirani[b]*, Vahid Vatanparast[c], Kazem Zavichi Turk[c], Mohamad Farooghi[d]

[a] *BSc, Department of Ceramic, Materials and Energy Research Center, Karaj, Iran.*
[b] *PhD, Department of Ceramic, Materials and Energy Research Center, Karaj, Iran.*
[c] *MSc, Faculty of Materials & Manufacturing Processes, Malek-e-Ashtar University of Technology, Tehran, Iran.*
[d] *MSc, Department of Materials Science and Engineering, Sharif University of Technology, Tehran, Iran.*

* Corresponding Author Email: m.shirani@merc.ac.ir (M. Shirani) URL: https://www.acerp.ir/article_238060.html

*ARTICLE INFO*

*Article History:*
Received: 29 May 2025
Revised: 09 September 2025
Accepted: 16 November 2025

*Keywords*:
Silicon Carbide (SiC),
Spark Plasma Sintering (SPS),
Additives,
Sintering,
Mechanical Properties

*ABSTRACT*

This study investigates the influence of metallic (Al, Ti + $H_3BO_3$) and oxide ($Al_2O_3$–$Y_2O_3$ and $Al_2O_3$–$Y_2O_3$–MgO–CaO) sintering aids on the densification behavior and mechanical properties of silicon carbide (SiC) consolidated by spark plasma sintering (SPS). The primary objective was to reduce the inherently high sintering temperature of SiC while maintaining or improving its mechanical performance. Experimental results demonstrate that appropriate additives significantly lower the sintering onset (as low as 1274 °C for SiC 5Al) and enable high final densities (relative densities >98%, e.g., 98.4% for SiC $3Al_2O_3$ $2Y_2O_3$) at overall sintering temperatures below 2000 °C. Among the formulations tested, SiC 10Al achieved a flexural strength of 417 MPa (97.2% relative density), whereas SiC $3Al_2O_3$ $2Y_2O_3$ exhibited a Vickers hardness of 29.6 GPa (98.4% relative density). Microstructural observations and phase analysis suggest that liquid-phase formation and additive–matrix interactions govern the observed densification and mechanical trends. These findings indicate that SPS combined with selected metallic or alumina–yttria-based additives represents an effective and industrially scalable route for fabricating dense, high-performance SiC components suitable for demanding applications in the energy, electronics, and automotive industries, as well as in wear-resistant tooling.

https:/doi.org/10.30501/acp.2025.526982.1177

## 1. INTRODUCTION

Advanced ceramics play a vital role in modern engineering and industrial applications owing to their remarkable hardness, low density compared with metals, and outstanding performance under extreme conditions (Anstis et al., 1981; Andraskar et al., 2022; Gooch, 2002). Among these, silicon carbide (SiC) stands out due to its exceptional mechanical strength, high thermal conductivity, and resistance to chemical attack. Depending on end use, SiC structures can be fabricated as monolithic ceramics or as composites incorporating compliant interlayers—such as aramid fibers, ultra high molecular weight polyethylene (UHMWPE), or lightweight metals like aluminum—to tailor their energy absorption capacity(Chen et al., 2024; David et al., 2009).

Unlike metals that absorb impact through plastic deformation, ceramics dissipate energy predominantly through microcracking and frictional bridging, aiding stress redistribution and suppressing catastrophic fracture(Flinders et al., 2005; Silveira et al., 2021). Structural integrity, density, porosity, and fracture

Please cite this article as: Falah M. R., Shirani, M., Vatanparast, V., Zavichi Turk, K. & Farooghi, M. (2025). The Effect of Metallic and Oxide Additives on Spark Plasma Sintering and Properties of Silicon Carbide Components, *Advanced Ceramics Progress*, 11(3), 01-12. https://doi.org/10.30501/acp.2025.526982.1177

toughness are therefore critical parameters for high performance ceramics used in aerospace,semiconductor, power, or protective sectors (Karandikar et al., 2009; Laible, 2012).

### 1.1. Sintering Challenges and SPS Advances

Pure or additive free SiC requires exceptionally high sintering temperatures—often approaching 2000–2200 °C—to reach near full theoretical density (Demirskyi et al., 2024). Although this range is slightly below conventional pressureless sintering limits (>2200 °C), it remains energy intensive and industrially impractical because of equipment constraints and grain coarsening (Zhou et al., 2003). The Spark Plasma Sintering (SPS) method mitigates these issues through electric field assisted mass transport, enabling rapid heating and short dwell times that yield fine grained dense SiC (Munir et al., 2006; Izhevskyi et al., 2000; She et al., 2017; Shaffer, 1969).

### 1.2. Oxide Additives and Liquid Phase Mechanisms

Oxide additives—particularly the $Al_2O_3$-$Y_2O_3$ system—are among the most effective sintering aids for SiC. These oxides generate low melting eutectics and react to form yttrium aluminum garnet ($Y_3Al_5O_{12}$, YAG), promoting viscous flow and liquid phase transport (Chen & Wang, 2000).

Chen et al. (2022) and Chai et al. (2021) confirmed accelerated densification via in situ YAG formation through mechanical alloying, aligning with the wetting and diffusional mechanisms described by Omori and Hirai (1997).

Marchi et al. (2006) and Munir et al. (2006) reported full densification around 1800 °C under 30 MPa for Al-Y-$SiO_2$ containing systems with enhanced strength relative to hot pressed samples.

Alternative rare earth oxides such as $Yb_2O_3$ also exhibit strong liquid phase sintering performance. Kim et al. (1998) noted densities near theoretical levels at 1750 °C (≈ 720 MPa strength; $K_{IC} \approx 4$ MPa·m$^{1/2}$) by SPS while Liu (1997) recorded > 99% density for AlN-$Y_2O_3$ systems near 1900 °C with oxidation resistance and nanograin refinement. Multi component oxide mixtures—MgO, CaO, and $Y_2O_3$—broaden liquid formation intervals, facilitating dense microstructures yet risking volatilization and residual porosity (Lee et al., 2012; Marchi et al., 2006).

Overall, densification results from the joint effects of low melting liquid formation (~1400–1800 °C), viscous YAG phase generation, $SiO_2$ removal, and boundary chemistry modification (Munir et al., 2006; Chen & Wang, 2000; Liu, 1997; Chai et al., 2021).

### 1.3. Metallic and Compound Additives

Metallic and reactive additives complement oxide systems, offering lower temperature routes toward dense SiC. Aluminum based additives and Al carbide intermediates such as $Al_4SiC_4$ are highly effective, enabling ~95% relative density at 1500 °C (Lee et al., 2012).

Shimoda (2018) achieved > 96% density at 1700 °C with Al coated nanopowders, yielding 592 MPa flexural strength and ≈ 5.4 MPa·m$^{1/2}$ toughness. Nevertheless, excess Al induces gas evolution and porosity (Prochazka, 1975; Pujar et al., 2000; Yamada et al., 1987). Omori and Hirai (1997), Izhevskyi et al. (2000), and Strecker et al. (1999) identified transient liquid phase formation that enhances wetting and densification in Al bearing SiC systems.

Beyond pure metals, ternary and reactive compound systems—particularly Al–B–C—show outstanding efficacy.

Lee (2011) obtained full density at 1525–1575 °C via SPS,achieving E ≈ 368 GPa and K_IC ≈ 4.7 MPa·m$^{1/2}$. Prochazka (1975) and Maître et al. (2008) elucidated boron's diffusional enhancement and carbon's oxygen control roles. However, excessive $B_4C$ inclusion can generate borosilicate phases and reduce microstructural homogeneity (Maître et al., 2008).

### 1.4. Titanium Based Reactive Systems

Titanium compounds significantly aid low temperature densification through in situ phase formation.

Podbolotov et al. (2015) attained 90-98% density and 550 MPa compressive strength at 1600-1700 ºC with $Ti_3SiC_2$ (MAX phase) formation.

Li et al. (2025) demonstrated that $TiB_2$ and TiC reinforced SiC composites exhibit enhanced fracture toughness because of crack deflection and bridging, consistent with Wang et al. (2013) observations on $TiB_2$ reinforced SiC processed by SPS. Such reactive systems thus achieve simultaneous densification and toughening through phase evolution at sub 2000 °C.

Integrating oxide, metallic, and composite additives enables concurrent mechanisms—viscous and liquid phase transport, intergranular reactions, and in situ reinforcement—that collectively lower the SPS sintering temperature of SiC below 2000 °C while maintaining fine grained, high strength microstructures. These results demonstrate the technological viability of multi additive SPS routes for industrial production of dense, tough, and thermally stable SiC based ceramics.

Finally, in the broader processing context, Munir et al. (2006) compared SPS, hot pressing, and pressureless sintering, concluding that SPS offers significantly shorter cycle times and reduced sintering temperatures due to field-assisted diffusion. These findings corroborate the temperature reductions and high densities achieved in the present study, underscoring the suitability of SPS for producing dense SiC bodies with tailored additive systems. This study focuses on evaluating the effectiveness of various commercially available metallic and oxide additives in lowering the SPS sintering temperature of SiC to below 2000 °C while achieving

high density and favorable mechanical properties. The aim is to identify additive systems and processing conditions suitable for industrial production.

## 2. MATERIALS AND METHODS

### 2.1 Materials

The primary material (Table 1) was commercially available granulated alpha-silicon carbide powder with an average particle size of 0.8 µm. The metallic additives investigated were aluminum (Al) and titanium (Ti), used in combination with boric acid ($H_3BO_3$). The oxide additives included aluminum oxide ($Al_2O_3$), yttrium oxide ($Y_2O_3$), magnesium oxide (MgO), and calcium carbonate ($CaCO_3$), the latter serving as a source of calcium oxide (CaO) upon decomposition. Ethanol and acetone were used as milling media.

### 2.2 Powder Preparation

Powder mixtures (Table 2) were prepared using a planetary ball mill. The ball-to-powder ratio (alumina balls with a diameter of 15–20 mm) was maintained at 3:1. For samples containing aluminum and titanium additives, acetone was used as the milling medium (100 cc per cup), and milling was carried out at 200 rpm for 1 hour. For samples containing oxide additives, ethanol was used as the milling medium (150 cc per cup), and milling was conducted at 300 rpm for 4 hours. After milling, the slurries were dried. The dried lumps were then crushed and sieved through a 45-mesh (355 µm) screen.

### 2.3 Spark Plasma Sintering (SPS)

The SPS process was carried out using a 100 kW unit with a maximum applied force of 10 tons. The process was primarily performed under mechanical pressure. Rectangular graphite molds with cavity dimensions of 50 × 17 × 45 mm were used.

A constant amount of 13.6 g of powder mixture was employed for each sample. The SPS process involved a heating rate of approximately 50 °C/min, with a mechanical pressure of 25 MPa applied during sintering. A holding time of 5 minutes was maintained at the final sintering temperature.

A layer of graphite foil (0.5 mm thick) was placed around the sample within the mold, and graphite felt (10 mm thick) was used as insulation. A schematic of the SPS device is shown in Figure 1.

Samples were placed inside the graphite chamber, which was then heated under vacuum. This enabled rapid feasibility studies. Based on these results, the optimal compositions were selected for further sintering in an industrial high-temperature graphite furnace under an argon atmosphere.

Based on the preliminary results, the selected compositions for detailed sintering experiments are summarized in Table 2.

**TABLE 1.** Particle size and chemical purity of the raw materials used in this study.

| Raw material | Average particle size (µm) | Purity (%) |
|---|---|---|
| Silicon carbide (SiC) | 0.8 | 99.0 |
| Aluminum (Al) | 2.0 | 99.0 |
| Titanium (Ti) | 20.0 | 99.0 |
| Boric acid ($H_3BO_3$) | — | 99.0 |
| Aluminum oxide ($Al_2O_3$) | 0.50 | 99.8 |
| Yttrium oxide ($Y_2O_3$) | 2.0 | 99.9 |
| Magnesium oxide (MgO) | 1.0 | 99.5 |
| Calcium carbonate ($CaCO_3$) | — | 99.0 |
| Ethanol | — | 99.8 |
| Acetone | — | 99.9 |

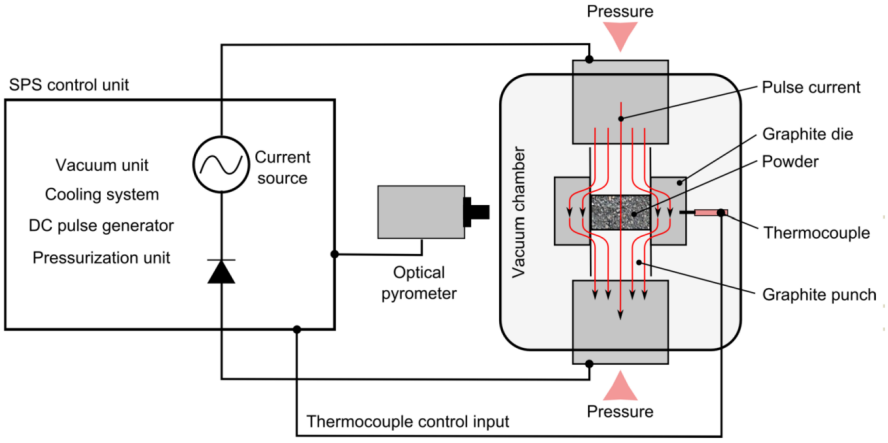


**Figure 1.** Spark Plasma Sintering (SPS) device in the pressure-assisted sintering mode.

**TABLE 2.** Sample designations and corresponding compositions (wt.%).

| Sample Code | SiC (wt.%) | Additives (wt.%) |
|---|---|---|
| SiC-5Al | 95 | 5% Al |
| SiC-10Al | 90 | 10% Al |
| SiC-Ti-$H_3BO_3$ | 98 | 1%Ti + 1$H_3BO_3$ |
| SiC-3A2Y | 95 | 3% $Al_2O_3$ + 2% $Y_2O_3$ |
| SiC-5A2Y | 93 | 5% $Al_2O_3$ + 2% $Y_2O_3$ |
| SiC-AYMC | 91 | )$Al_2O_3$+$Y_2O_3$+MgO +CaO(9% |

### 2.4 Characterization

After SPS processing under mechanical pressure, the sintered specimens were carefully extracted from the graphite molds. Residual graphite coating on the sample surfaces was removed by precision grinding to prepare them for subsequent characterization.

**Density and Apparent Porosity:** Bulk density and apparent porosity were measured according to ASTM C373 using the Archimedes method. Samples were boiled in distilled water for 5 hours, soaked for 24 hours, and weighed dry, saturated, and suspended to calculate bulk density (B) and apparent porosity (%P) using the formulas:

$$\%P = \left[\frac{(W - D)}{(W - S)}\right] \times 100 \quad (1)$$

$$B = \frac{D}{(W-S)} \quad (2)$$

where D is dry weight, W is saturated weight, and S is suspended weight.

**Flexural Strength:** Three-point flexural strength was measured on samples with dimensions of approximately 50 × 4 × 3 mm. The support span was 40 mm, and the upper loading pin had a diameter of 2 mm. A loading speed of 0.5 mm/min was used. Flexural strength (S) was calculated using the formula: $S = 3PL / 2bd^2$ where P is the fracture load (N), L is the support span (mm), b is the sample width (mm), and d is the sample thickness (mm). The reported value is the average of three samples.

**Microhardness:** Vickers microhardness was measured using an Akashi MVK-H21 device according to ASTM E384. Samples were polished to 5000 mesh. A load of 200 gf (1.96 N) was applied for 15 seconds. Vickers microhardness was calculated as the average of five indentations using the formula: $HV = 0.0018544\ P/d^2$ where P is the applied load (N) and d is the average diagonal length of the indentation (mm). Hardness values were converted to GPa.

**Fracture Toughness:** Fracture toughness (KIC) was estimated using the Vickers indentation method with crack length measurement. Although this method is not yet standardized, it is commonly applied for SiC according to the literature. Samples were polished to 5000 mesh before testing. A load of 10 kgf (98 N) was applied for 15 seconds to create indentations with measurable cracks. KIC was calculated using the formula proposed by Anstis et al.: $KIC = 0.016[E/HV]^{0.5}\ [P/c^{1.5}]$ where E is the Young's modulus (400 GPa for SiC), $H_V$ is the Vickers hardness (GPa), P is the applied load (N), and c is the average distance from the center of the indentation to the crack tip (mm). Crack lengths were measured using an optical microscope at 200x magnification [13].

**X-ray Diffraction (XRD):** XRD analysis was performed to identify the phases present in the initial powder and sintered samples.

**Scanning Electron Microscopy (SEM) and Energy-Dispersive X-ray Spectroscopy (EDS):** SEM was used to observe the morphology of the initial powders and the microstructure of sintered samples. EDS was used for elemental analysis.

## 3. RESULTS AND DISCUSSION

### 3.1 Initial Powder Characterization and Feasibility Samples

The initial granulated alpha-SiC powder had an average particle size of 0.8 µm. SEM images (Figure 2(a) and (b)) showed that the powder consisted of granules smaller than 200 µm, with individual particles within the granules being smaller than 2 µm. EDS analysis indicated approximately 5.5 atomic percent oxygen in the initial powder (Figure 2(c)).

Feasibility disk samples (10 mm diameter) were pressed from the initial granulated powder at 50 MPa and 150 MPa, resulting in green densities of 41% and 51%, respectively. After milling the granulated powder for 1 hour at 200 rpm, the green density of pressed samples (at 120 MPa) increased to approximately 54%.

This indicates that breaking up the granules and achieving a higher initial density in the green body improves compaction. SPS of the initial granulated powder without additives at 1800 °C and 1850 °C resulted in bulk densities of 2.89 g/cm³ and 2.92 g/cm³, respectively, corresponding to relatively low densification without effective additives. During SPS, significant gas release was observed between 200 and 600 °C, potentially due to the resin additive in the initial powder. XRD analysis of the initial granulated powder showed alpha-SiC, primarily of the 6H and 5H polytypes. After sintering at high temperatures, some 4H-SiC and graphite were detected, indicating that the resin present in the commercial powder pyrolyzes at high temperatures, with the resulting carbon graphitizing

during sintering (Figure 3 shows the XRD patterns of the initial powder and a sintered sample).

### 3.2 SPS Sintered Samples

Rectangular samples with various additives were sintered using SPS under a mechanical pressure of 25 MPa (Figure 4). Samples containing titanium and boric acid exhibited a different surface polish compared to the others, possibly due to secondary phase formation. For aluminum-containing samples, successful removal from the mold became difficult at 15 wt% Al, suggesting excessive liquid-phase formation or reactions. The sintering behavior was monitored through displacement, temperature, and time curves during SPS.

These curves enabled the determination of the sintering start temperature and the final sintering temperature (see Figures 5-7, and Table 3 for representative displacement–temperature–time curves for different compositions). The sintering behavior of the prepared SiC-based specimens was evaluated based on the onset and final sintering temperatures as well as the resulting relative densities determined by the Archimedes method. The summarized results are presented in Table 3.

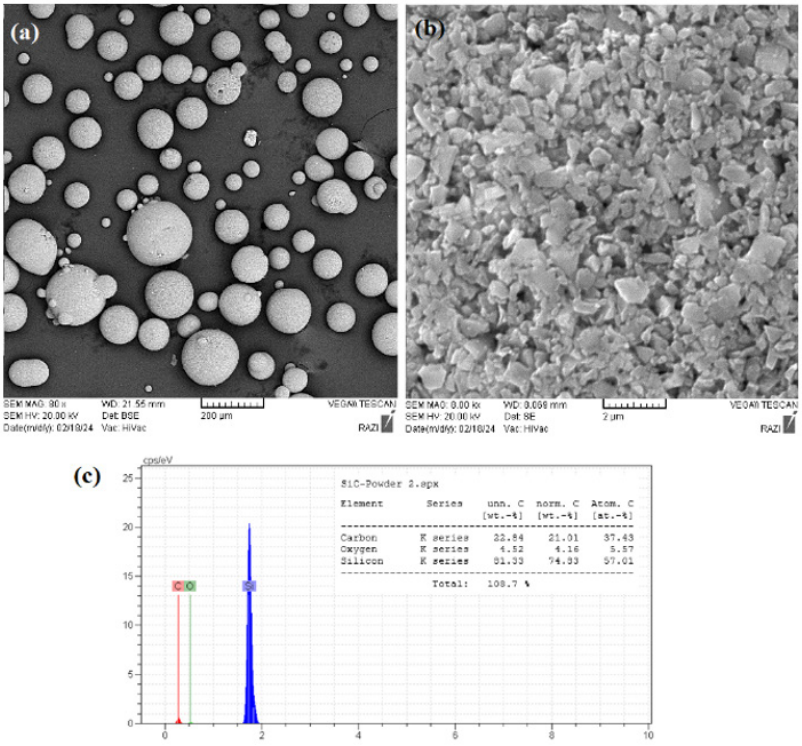


**Figure 2.** SEM images of SiC powder at magnifications of (a) 80×, (b) 8000×, and (c) EDS analysis.

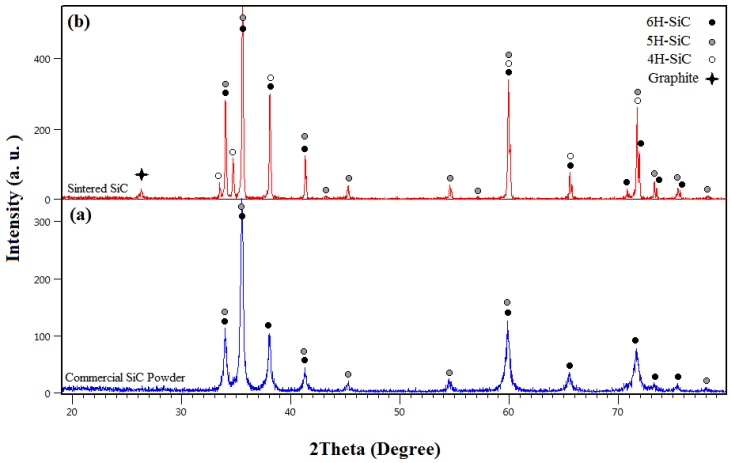


**Figure 3.** XRD patterns of (a) the initial powder and (b) the sample sintered at 1950 °C using the SPS method.


**Figure 4.** Rectangular samples fabricated via SPS with different compositions**.**

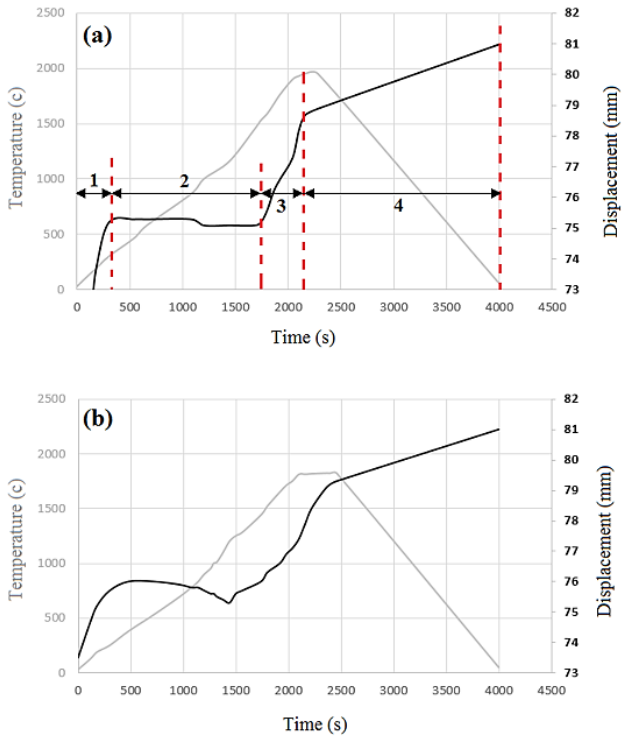


**Figure 5.** Displacement and temperature versus time plots during sintering for (a) the initial commercial granules and (b) the milled granules.

**TABLE 3.** Sintering onset temperature, final sintering temperature, and relative density of SiC specimens with various additive systems, measured by the Archimedes method (mean values from three replicates)

| Sample | Sintering Onset Temp. (°C) | Final Sintering Temp. (°C) | Relative Density (%) |
|---|---|---|---|
| Granule | 1530 | 1950 | 99.1 |
| Milled | 1480 | 1950 | 98.8 |
| SiC–5Al | 1274 | 1830 | 98.1 |
| SiC–10Al | 1330 | 1880 | 97.2 |
| SiC–Ti–$H_3BO_3$ | 1390 | 2080 | 93.8 |
| SiC–3$A_2$Y | 1420 | 1900 | 98.4 |
| SiC–5$A_2$Y | 1380 | 1800 | 98.1 |
| SiC–AYMC | 1365 | 1790 | 95.0 |

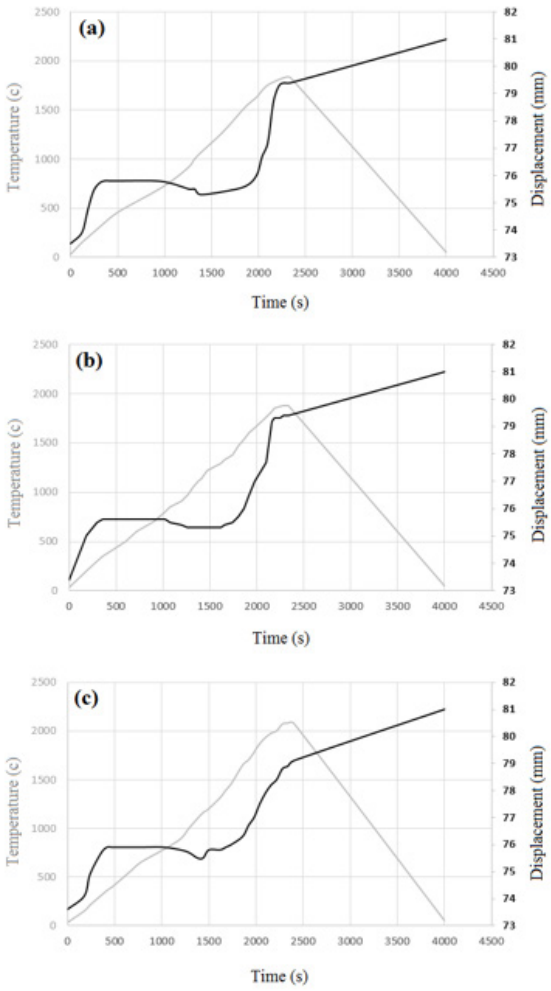


**Figure 6.** Displacement and temperature versus time profiles during sintering of (a) SiC-5Al, (b) SiC-10Al, and (c) SiC-Ti-$H_3BO_3$ samples.

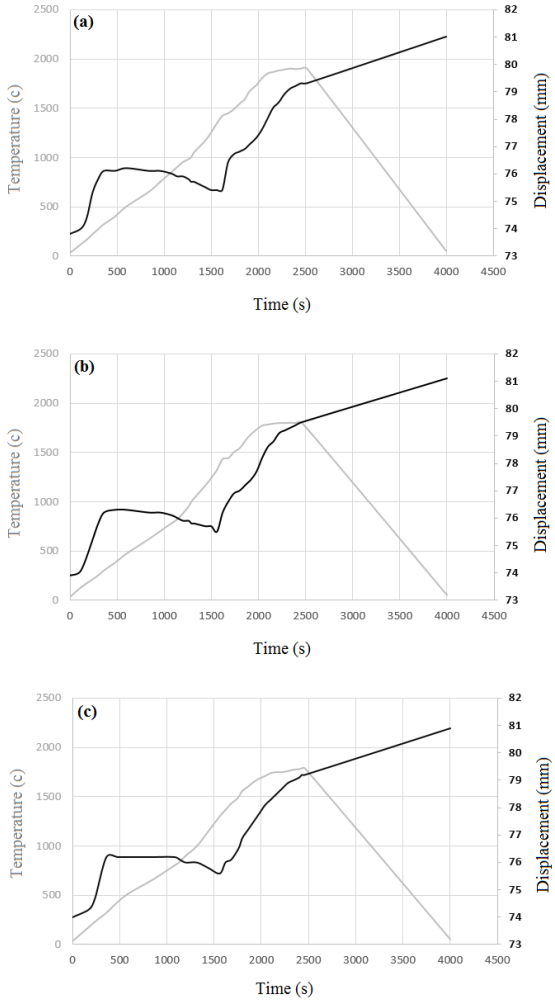


**Figure 7.** Displacement and temperature versus time profiles during sintering of (a) SiC-3A2Y, (b) SiC-5A2Y, and (c) SiC-AYMC samples.

Metallic aluminum additives effectively reduced both the sintering start and final temperatures compared to pure milled SiC. For SiC-5Al, the start temperature was 1274 °C and the final temperature was 1819 °C, while for SiC-10Al, the start was 1330 °C and the final temperature was 1880 °C, both lower than those of milled SiC (1480 °C start, 1950 °C final).

The titanium- and boric acid-containing system (SiC-Ti-H3BO3) also showed a reduced sintering start temperature (1390 °C), but the final temperature (2080 °C) was higher than that of pure milled SiC. The achieved density was relatively low (93.8%), indicating that this system was not successful in achieving high density under these conditions, potentially due to coarse initial Ti powder or inadequate mixing.

Oxide additives also significantly lowered the sintering start temperature. For SiC-3A2Y, the start temperature was 1420 °C (higher than some other systems but still below the final temperature), and the final temperature was 1900 °C. For SiC-5A2Y, the start was 1380 °C and the final temperature was 1800 °C. The AYMC system (Alumina–Yttria–Magnesium Oxide–Calcium Oxide) showed a start temperature of 1365 °C and a final temperature of 1790 °C, but did not achieve high density (95%), possibly due to the tested temperature being too high, leading to evaporation of low-melting compounds.

XRD analysis of the Al-containing samples confirmed the presence of metallic Al peaks after milling and drying, indicating that aluminum did not undergo significant oxidation during powder preparation (Figures 8–10). Observations suggested that increasing the temperature in Al-containing samples led to macroscopic porosity. Cracks were also observed in the SiC-10Al sample, possibly related to the high Al content and formation of Al–SiC reaction products.

The as-received α-SiC powder (Figure 8a) exhibits sharp diffraction peaks corresponding to the 6H and 5H

polytypes, with no significant secondary phases. After ball milling with 5 wt% and 15 wt% Al (Figures 8b and 8c), characteristic FCC aluminum reflections emerge alongside SiC peaks, confirming that the metallic state of Al is retained during powder preparation. Slight peak broadening of SiC in the milled blends suggests reduced crystallite size, a factor known to accelerate sintering via enhanced mass transport (Munir et al., 2006). Similar to earlier studies, this solid-state preservation of metallic Al provides a low-temperature liquid phase upon heating, initiating densification below 1300 °C. In the SPS-processed SiC–5Al sample (Figure 9a), metallic Al peaks were absent, replaced by strong reflections of $Al_4C_3$ and minor $Al_2O_3$, indicating active reactions between Al and SiC during heating. The SiC–10Al specimen (Figure 9b) exhibited more intense $Al_4C_3$ peaks and probable Al–Si–C intermediates (e.g., $Al_8SiC_7$), consistent with a higher liquid-phase fraction and enhanced grain-boundary wetting. However, as reported by Kim and Kim (2019), the formation of $Al_4C_3$ can embrittle the microstructure. This agrees with our observation of microcracks in SiC–10Al, despite its peak flexural strength (417 MPa), and highlights the well-known hardness–strength trade-off in liquid-phase-sintered SiC.

The SiC–$3Al_2O_3$–$2Y_2O_3$ composition (Figure 10a) shows distinct yttrium aluminum garnet ($Y_3Al_5O_{12}$, YAG) peaks alongside α-SiC. At 5 wt% $Al_2O_3$ (Figure 10b), YAG peak intensities increase, indicating more extensive liquid-phase formation. Both compositions achieved relative densities above 98%, consistent with findings by Kim and Kim (2019), where YAG-containing SiC reached approximately 98.8% density at 1800 °C under pressureless sintering. In the AYMC composite (Figure 10c), peaks of YAG, $MgAl_2O_4$ spinel, and $CaSiO_3$ are detected.

The multicomponent system promotes a complex network of liquid phases; however, partial volatilization of MgO and CaO at the applied SPS temperatures likely generated closed porosity, reducing the density to approximately 95%. This porosity effect, also noted in the reference study, explains the corresponding reduction in hardness and flexural strength observed in our samples.

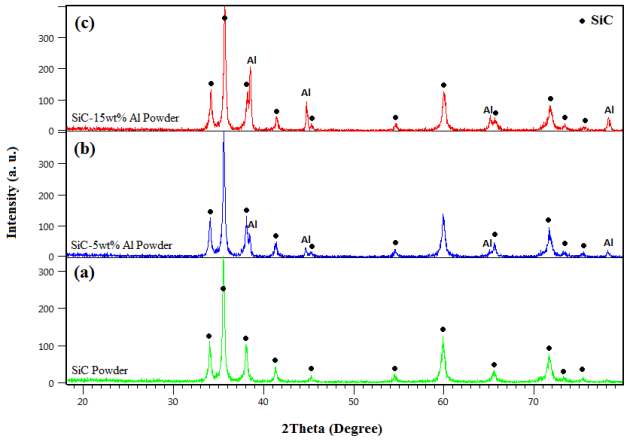


**Figure 8.** XRD patterns of (a) the initial powder, (b) ball-milled SiC-5Al powder mixture, and (c) ball-milled SiC-15Al powder mixture.

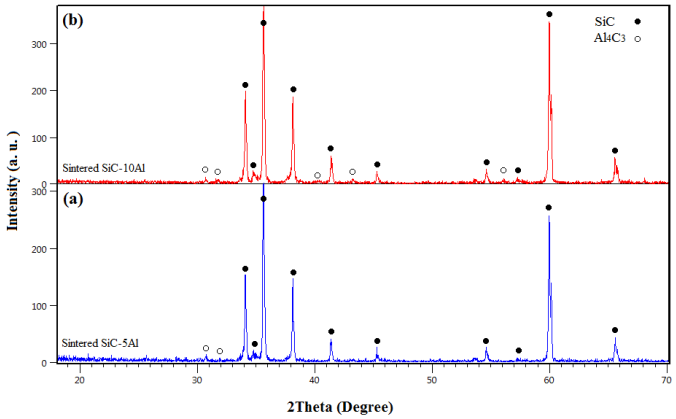


**Figure 9.** XRD patterns of aluminum-containing samples after SPS processing: (a) SiC-5Al and (b) SiC-10Al.

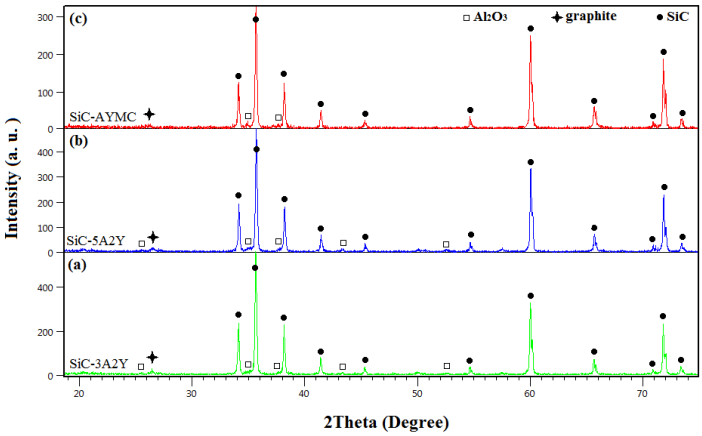


**Figure 10.** XRD patterns of samples containing oxide sintering aids after SPS processing: a) SiC-3$Al_2O_3$-2$Y_2O_3$,b) SiC-5$Al_2O_3$-2$Y_2O_3$,c) SiC-$Al_2O_3$+$Y_2O_3$+MgO+CaO

The SEM observations in Figure 11 highlight the pronounced influence of metallic and oxide additives on the microstructural development of SPS-processed SiC composites. The SiC–5Al sample exhibits a tightly packed, uniform arrangement of equiaxed grains with clean boundaries, consistent with its high relative density (98.1%). Thin secondary phases are visible along some grain boundaries, likely associated with Al–SiC reaction products formed during sintering.

In contrast, the SiC–Ti–$H_3BO_3$ composite shows conspicuous intergranular pores and a less compact structure, correlating with its lower density (93.8%). This morphology suggests incomplete densification and the possible formation of undesirable phases such as $TiB_2$ or $TiO_2$ due to non-optimal reaction pathways.

The oxide-modified systems demonstrate more favorable densification. The SiC–3$Al_2O_3$–2$Y_2O_3$ and SiC–5$Al_2O_3$–2$Y_2O_3$ composites both contain fine grains bounded by thin intergranular films, likely yttrium–aluminum garnet (YAG) or glassy phases, contributing to enhanced mechanical properties (98.4% and 98.1% density, respectively). The increased oxide content in the latter appears to promote more extensive liquid-phase formation, leading to slightly finer grain sizes.

By contrast, the multicomponent AYMC system exhibits a less uniform microstructure with greater porosity (95% density), a condition most likely caused by the volatilization of low-melting constituents during high-temperature sintering. This microstructural feature is consistent with the measured reduction in its mechanical performance.

### 3.3 Physical and Mechanical Properties

The physical and mechanical properties of selected SPS-sintered samples are presented in Table 4. Comparing milled SiC (98.8% density, 251 MPa flexural strength, 28.9 GPa hardness, 2.9 MPa√m toughness) with samples containing additives, several systems exhibited improved properties, particularly in density and hardness.

The SiC–5Al sample achieved 98.1% density with 280 MPa flexural strength, 23.5 GPa hardness, and 4.1 MPa√m toughness. SiC–10Al reached 97.2% density, 417 MPa strength, 24.6 GPa hardness, and 3.6 MPa√m toughness. The increase in Al content led to higher strength and toughness, although hardness decreased slightly. The SiC–Ti–$H_3BO_3$ sample, despite a lower sintering start temperature, exhibited a low final density (93.8%) and consequently poorer flexural strength (318 MPa) and toughness (3.1 MPa√m), although hardness remained relatively high (27.7 GPa).

Among the oxide systems, SiC–3A2Y reached 98.4% density, 297 MPa strength, 29.6 GPa hardness, and 3.3 MPa√m toughness. SiC–5A2Y achieved a high density (98.1%) with 309 MPa strength, 28.3 GPa hardness, and 3.2 MPa√m toughness. The AYMC sample, as noted, had lower density (95%) and consequently lower properties (339 MPa strength, 24.8 GPa hardness, 2.7 MPa√m toughness). Overall, the results demonstrate that metallic aluminum and the tested oxide systems ($Al_2O_3$–$Y_2O_3$) are effective sintering aids for SiC via SPS, enabling high densification at temperatures below 2000 °C. High density was achieved in several compositions, generally correlating with improved mechanical properties such as flexural strength and hardness. Fracture toughness varied depending on the additive system and, potentially, the resulting microstructure and secondary phases. The lower density of the AYMC system suggests that the tested temperature was not optimal for this specific composition. The physical and mechanical characteristics of the selected SPS-sintered SiC specimens were determined based on their density, flexural strength, microhardness, hardness, and fracture toughness. The mean values obtained from three replicate measurements are summarized in Table 4.

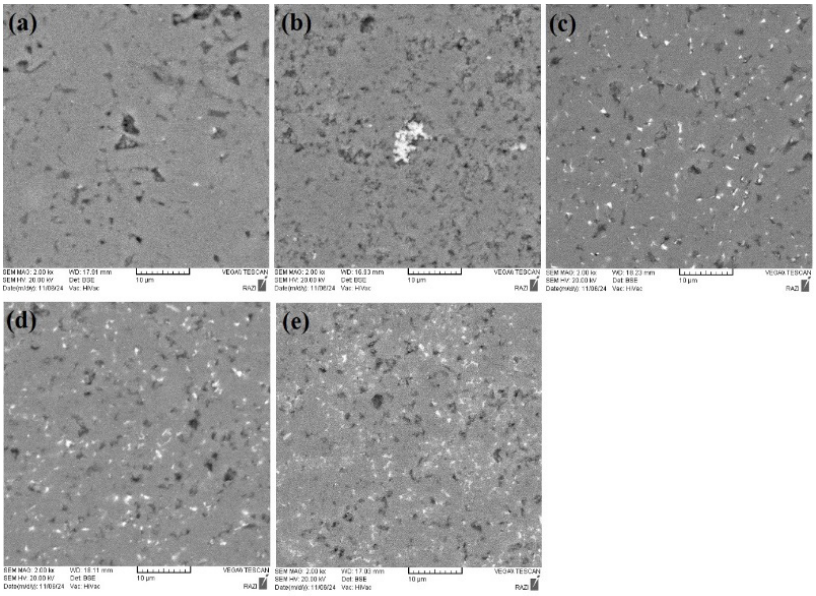


**Figure 11.** SEM images of (a) SiC-5Al, (b) SiC-Ti- $H_3BO_3$, (c) SiC-3$Al_2O_3$-2$Y_2O_3$, (d) SiC-5$Al_2O_3$-2$Y_2O_3$ and (e) SiC-9($Al_2O_3$+$Y_2O_3$+MgO+CaO)

**TABLE 4.** Physical and mechanical properties of selected SPS-sintered SiC samples. Values are based on three replicate specimens.

| Sample | Relative Density (%) | Flexural Strength (MPa) | Microhardness ($H_V$) | Hardness (GPa) | Fracture Toughness (MPa$\sqrt{m}$) |
|---|---|---|---|---|---|
| Granule | 99.1 | 330 ± 59 | 2920 ± 109 | 28.6 ± 1.1 | 2.5 ± 0.1 |
| Milled | 98.8 | 251 ± 35 | 2947 ± 24 | 28.9 ± 0.2 | 2.9 ± 0.4 |
| SiC – 5Al | 98.1 | 280 ± 17 | 2396 ± 118 | 23.5 ± 1.7 | 4.1 ± 0.5 |
| SiC – 10Al | 97.2 | 417 ± 62 | 2511 ± 76 | 24.6 ± 0.7 | 3.6 ± 0.2 |
| SiC – Ti – $H_3BO_3$ | 93.8 | 318 ± 43 | 2821 ± 130 | 27.7 ± 1.3 | 3.1 ± 0.4 |
| SiC – 3Al2Y | 98.4 | 297 ± 41 | 3216 ± 62 | 29.6 ± 0.6 | 3.3 ± 0.4 |
| SiC – 5Al2Y | 98.1 | 309 ± 12 | 2890 ± 147 | 28.3 ± 1.4 | 3.2 ± 0.2 |
| SiC – AYMC | 95.0 | 339 ± 7 | 2530 ± 50 | 24.8 ± 0.5 | 2.7 ± 0.1 |

## 4. CONCLUSION(S)

This study clearly demonstrates that incorporating selected metallic (Al, Ti + $H_3BO_3$) and oxide ($Al_2O_3$–$Y_2O_3$, $Al_2O_3$–$Y_2O_3$–MgO–CaO) additives enables near-full densification of silicon carbide (SiC) via Spark Plasma Sintering (SPS) at temperatures well below 2000 °C. The findings highlight the strong influence of additive selection on sintering kinetics, densification, and the resulting mechanical performance.

The principal outcomes are as follows:

- Both metallic aluminum and alumina–yttria-based oxide additives proved highly effective, lowering the sintering onset temperature to 1274 °C and achieving near-full densification at final temperatures of 1800–1900 °C.
- The SiC–10Al composition exhibited a well-balanced property profile, attaining 97.2 % relative density alongside a flexural strength of 417 MPa.
- Within the oxide systems, the SiC–3$Al_2O_3$–2$Y_2O_3$ composition delivered a Vickers hardness of 29.6 GPa with 98.4 % relative density, reaffirming the effectiveness of $Al_2O_3$–$Y_2O_3$ as a potent liquid-phase sintering aid.
- The Ti + $H_3BO_3$ and multicomponent $Al_2O_3$–$Y_2O_3$–MgO–CaO systems did not achieve full densification under the employed processing conditions, most likely due to suboptimal parameters or volatilization of low-melting constituents.

Overall, the results confirm that judiciously designed additive systems—particularly those based on aluminum and $Al_2O_3$–$Y_2O_3$—offer a robust pathway for producing dense, high-performance SiC ceramics at substantially reduced SPS temperatures. This approach holds considerable promise for large-scale manufacturing of advanced structural components, including ceramic armor and other applications demanding exceptional mechanical performance.

## NOMENCLATURE

| | |
|---|---|
| SPS | Spark Plasma Sintering |
| SiC | Silicon Carbide |
| Al | Aluminum |
| Ti | Titanium |
| $H_3BO_3$ | Boric acid |
| $Al_2O_3$ | Aluminum oxide |
| $Y_2O_3$ | Yttrium oxide |
| MgO | Magnesium oxide |
| CaO | Calcium oxide |
| YAG | Yttrium–Aluminum Garnet |
| $\rho_r$ | Relative density (%) |
| $T_o$ | Sintering onset temperature (°C) |
| $T_e$ | Final sintering temperature (°C) |
| Hv | Vickers microhardness |
| $\sigma_f$ | Flexural strength (MPa) |
| K_IC | Fracture toughness (MPa√m) |
| SEM | Scanning Electron Microscopy |
| EDS | Energy Dispersive X-ray Spectroscopy |
| XRD | X-ray Diffraction |
| FCC | Face-Centered Cubic |
| ASTM | American Society for Testing and Materials |
| SPS–95SiC–5Al | Sample with 95 wt.% SiC and 5 wt.% Al |
| SPS–90SiC–10Al | Sample with 90 wt.% SiC and 10 wt.% Al |
| SPS–98SiC–Ti–$H_3BO_3$ | Sample with 98 wt.% SiC, 1 wt.% Ti, and 1 wt.% $H_3BO_3$ |
| SPS–93SiC–5A2Y | Sample with 93 wt.% SiC, 5 wt.% $Al_2O_3$, and 2 wt.% $Y_2O_3$ |
| SPS–91SiC–AYMC | Sample with 91 wt.% SiC and mixed oxides ($Al_2O_3$–$Y_2O_3$–MgO–CaO) |
| B | Bulk density |
| %P | Apparent porosity |
| EE | Electrical energy input during SPS |
| MPa | Megapascal |
| °C | Degree Celsius |

## REFERENCES


1. Andraskar, N. D., Tiwari, G., & Goel, M. D. (2022). Impact response of ceramic structures—A review. *Ceramics International*, 48(19), 27262–27279. https://doi.org/10.1016/j.ceramint.2022.06.313
2. Anstis, G. R., Chantikul, P., Lawn, B. R. & Marshall, D. B.(1981. A critical evaluation of indentation techniques for measuring fracture toughness: I, direct crack measurements. *Journal of the American Ceramic Society*, 64(9), 533–538. https://doi.org/10.1111/j.1151-2916.1981.tb10320.x
3. Anya, C. C. (1999). Microstructural nature of strengthening and toughening in $Al_2O_3$–SiC(p) nanocomposites. *Journal of Materials* Science, 34(22), 5557–5567. https://doi.org/10.1023/A:1004729015686
4. Chai, Z., Gao, Z., Liu, H., et al. (2021). Thermal conductivity of SPS SiC ceramics with $Al_2O_3$ and $Y_2O_3$. *Journal of the European Ceramic Society*, 41(6), 3471–3479. https://doi.org/10.1016/j.jeurceramsoc.2020.12.020
5. Chen, I. W., & Wang, X. H. (2000). Sintering dense nanocrystalline ceramics without final stage grain growth. *Nature*, 404(6774), 168–171 https://doi.org/10.1038/35004548
6. Chen, R., Bratten, A., Rittenhouse, J., & Wen, H. (2022). Effects of mechanically alloying $Al_2O_3$ and $Y_2O_3$ additives on the liquid phase sintering behavior and properties of SiC. *Ceramics International*, 48(21), 31679–31685. https://doi.org/10.1016/j.ceramint.2022.07.089
7. Chen, Y.-L., Chu, C.-K., Chen, Y.-Z., & Liu, S.-C. (2024). Ballistic resistance of silicon-carbide-based ceramic and ultrahigh-molecular-weight polyethylene composite armor. *Transactions of the Indian Ceramic Society*, 83(2), 69–82. https://doi.org/10.1080/0371750X.2024.2307622
8. David, N. V., Gao, X. L., & Zheng, J. Q. (2009). Ballistic resistant body armor: Contemporary and prospective materials and related protection mechanisms. *Journal of Applied Mechanics*, 76(3), 031009. https://doi.org/10.1115/1.3124644
9. Demirskyi, D., Sepehri Amin, H., & Vasylkiv, O. (2024). High temperature deformation and consolidation of α-SiC by SPS. *International Journal of Applied Ceramic Technology.* https://doi.org/10.1111/ijac.14967
10. Flinders, M., Ray, D., Anderson, A., & Cutler, R. A. (2005). High-toughness silicon carbide as armor. *Journal of the American Ceramic Society*, 88(8), 2217–2226. https://doi.org/10.1111/j.1551-2916.2005.00415.x
11. Gooch, W. A. (2002). An overview of ceramic armor applications. *Ceramic Transactions*, 134, 3–21. https://www.researchgate.net/publication/286149363
12. Izhevskyi, V. A., Genova, L. A., Bressiani, J. C., & Bressiani, A. H. A. (2000). Silicon carbide: Structure, properties and processing. *Cerâmica*, 46, 4–13. https://doi.org/10.1590/S0366-69132000000100002
13. Karandikar, P. G., Evans, G., Wong, S., Aghajanian, M. K., & Sennett, M. (2009). A review of ceramics for armor applications. *Advances in Ceramic Armor IV*, 29, 163–175. https://doi.org/10.1002/9780470456286.ch16
14. Kim, Y. W., Mitomo, M., Emoto, H., & Lee, J. G. (2005). Effect of initial α-phase content on microstructure and mechanical properties of sintered SiC. *Journal of the American Ceramic Society*, 81(12), 3136–3140. https://doi.org/10.1111/j.1151-2916.1998.tb02748
15. Lee, J. S., Ahn, Y. S., Nishimura, T., Tanaka, H., & Lee, S. H. (2012). Effect of $Al_4SiC_4$ additive on β-SiC densification under vacuum. *Journal of the European Ceramic Society*, 32(3), 619–625. https://doi.org/10.1016/j.jeurceramsoc.2011.10.003
16. Lee, S. H. (2011). Low-temperature sintering of sub micro meter scale SiC using spark plasma sintering. *Journal of the Ceramic Society of Japan*, 119(1392), 640–643. https://doi.org/10.2109/jcersj2.119.640
17. Li, Z., Ren, Y., & Tan, C. (2025). Influence of TiB and TiC on structural integrity of Ti composites during dynamic deformation. *Materials Characterization*, 115374. https://doi.org/10.1016/j.matchar.2025.115374
18. Liu, D. M. (1997). Oxidation of polycrystalline α-SiC ceramic. *Ceramics International*, 23(5), 425–436. https://doi.org/10.1016/S0272-8842(96)00051-X
19. Maître, A. V. P. A., Vande Put, A., Laval, J. P., Valette, S., & Trolliard, G. (2008). Role of boron on the SPS of α-SiC powder. *Journal of the European Ceramic Society*, 28(9), 1881–1890. https://doi.org/10.1016/j.jeurceramsoc.2008.01.002
20. Marchi, J., Bressiani, J. C., & Bressiani, A. H. A. (2006). Sintering of SiC ceramics with ($Y_2O_3$–$Al_2O_3$–$SiO_2$) additives. *dvances in Science and Technology*, 45, 1739–1744. https://doi.org/10.4028/www.scientific.net/AST.45.1739
21. Munir, Z. A., Anselmi-Tamburini, U., & Ohyanagi, M. (2006). The effect of electric field and pressure on the synthesis and consolidation of materials: A review of the spark plasma sintering method. *Journal of Materials Science*, 41(3), 763–777. https://doi.org/10.1007/s10853-020-05040-4
22. Shaffer, P. T. B. (1969). A review of the structure of silicon carbide. *Acta Crystallographica Section B: Structural Science*, 25(3), 477–488. https://doi.org/10.1107/S0567740869002457
23. She, X., Huang, A. Q., Lucia, O., & Ozpineci, B. (2017). Review of silicon carbide power devices and their applications. *IEEE Transactions on Industrial Electronics*, 64(10), 8193–8205. https://doi.org/10.1109/TIE.2017.2652401
24. Shimoda, K. (2018). Low-temperature SPS of SiC nanopowder with Al layer. *Journal of the Ceramic Society of Japan*, 126(10), 757–762. https://doi.org/10.4416/jcst2018-00035

25. Silveira, P. H. P. M. D., Silva, T., Ribeiro, M. P., Rodrigues de Jesus, P., Credmann, P. C. R. D. S., & Gomes, A. (2021). A brief review of alumina, silicon carbide and boron carbide ceramic materials for ballistic applications. *Academia Letters*, 3742, 1–11. https://doi.org/10.20935/AL3742

26. Strecker, K., Ribeiro, S., Camargo, D., Silva, R., Vieira, J., & Oliveira, F. (1999). Liquid-phase sintering of silicon carbide with $AlN/Y_2O_3$, $Al_2O_3/Y_2O_3$ and $SiO_2/Y_2O_3$ additions. *Materials Research*, 2, 249–254. https://doi.org/10.1590/S1516-14391999000400003

27. Yamada, O., Miyamoto, Y., & Koizumi, M. (1987). Self-propagating high-temperature synthesis of SiC. *Journal of Materials Research*, 2(2), 275–278. https://doi.org/10.1557/JMR.1986.0275

28. Zhou, Y., Hirao, K., Yamauchi, Y., & Kanzaki, S. (2003). Densification and grain growth in pulse electric current sintering of alumina. *Journal of the European Ceramic Society*, 23(10), 1697–1701. https://doi.org/10.1016/j.jeurceramsoc.2003.10.013